Formation of monolayer charge density waves and anomalous edge doping in Na doped bulk VSe_2

Ulysse Chazarin, Mahé Lezoualc'H, Jyh-ping Chou, Woei Wu Pai, Abhishek Karn, Raman Sankar, Cyril Chacon, Yann Girard, Vincent Repain, Amandine Bellec, et al.

Formation of monolayer charge density waves and anomalous edge doping in Na doped bulk VSe_2

U. Chazarin M. Lezoualc'h J.P. Chou Woei Wu Pai A. Karn R. Sankar C. Chacon Y. Girard V. Repain A. Bellec S. Rousset A. Smogunov Y. J. Dappe J. Lagoute

U. Chazarin, C. Chacon, Y. Girard, V. Repain, A. Bellec, A. Rousset, J. Lagoute
Laboratoire Matériaux et Phénomènes Quantiques, CNRS-Université Paris Cité, 10 rue Alice Domon et Léonie Duquet, 75205 Paris Cedex 13, France.
jerome.lagoute@u-paris.fr
U. Chazarin, Woei Wu Pai, A. Karn
Center for Condensed Matter Science (CCMS), National Taiwan University, 11106 Taipei, Taiwan, ROC
wpai@ntu.edu.tw
M. Lezoualc'h, A. Smogunov, Y. J. Dappe
SPEC, CEA, CNRS, Université Paris-Saclay, CEA Saclay, 91191 Gif-sur-Yvette Cedex, France
J.P. Chou
Department of Physics, National Changhua University of Education, Chuanghua City, 50007
R. Sankar
Institute of Physics, Academia Sinica, Nankang, Taipei 11529, Taiwan

Keywords: *Scanning Tunneling Microscope, Transition Metal Dichalcogenides, VSe_2, Electrostatic effect*

Alkali atom doping is an efficient way to induce charge transfer and Fermi level tuning in layered materials through intercalation. However, there is a general lack of microscopic understanding of the effect of doping inhomogeneity in geometric and electronic aspects. Here we report surface doping of a bulk VSe_2 crystal by sodium. Na atoms form intercalated subsurface islands that modify the electronic phase of the top layer of VSe_2. In addition to n-doping, the charge density wave of the intercalated VSe_2 surface layer changes from the (4×4) bulk phase to the ($\sqrt{3} \times \sqrt{7}$) known in monolayer phase of VSe_2. Surprisingly, an electronic state at the edges of Na-intercalated area shift anomalously upward in energy as detected by scanning tunneling spectroscopy. This is explained by a local gating effect resulting from local dipoles at the edges. Our study illustrates a clear example of intercalation effect that should be general in alkali-intercalated bulk layered materials.

1 Introduction

Layered materials such as transition metal dichalcogenides (TMDs) can exhibit different physical properties depending on the number of layers. The electronic transition from bulk to few-layers or monolayer offers a rich playground for fundamental physics and applications. Metallic TMDs have generated a wide research interest since they can undergo various phase transitions including charge density waves (CDW). The control of CDW phases can be exploited for various applications such as oscillators [1] and data storage [2]. Although the CDW phenomenon is well understood in 1D systems, its origin in 3D and 2D materials is still much discussed [3]. In the TMD family, 1T-VSe_2 is of potential interest for different applications such as photodetection [4], electrocatalysis [5], as well as alkali ion storage [6]. 1T-VSe_2 is also particularly intriguing in many aspects. In its bulk form, it exhibits a three-dimensional $4 \times 4 \times 3$ CDW below 120 K for which different mechanisms such as Fermi surface nesting or electron-phonon coupling [7] [8], [9], have been proposed. In monolayer VSe_2, the CDW transition temperature nearly doubles to 220 K and the CDW adopts another unique symmetry [10]. Recently, possible ferromagnetism in monolayer 1T-VSe_2 has been reported and it is subjected to debate with possible evidence of defect induced magnetism [11, 12, 13, 14, 15]. The sensitivity of VSe_2 to defects or interlayer interactions allows to envisage methods of tuning its properties by external perturbations. It has been shown that the d band filling of the TMD metal cations, can play a key role in the CDW phase . Therefore interaction of VSe_2 with charge dopants can be a promising route to tune its electronic properties.
Elemental alkali are efficient dopants since they are strong electron donors. Their interactions with TMDs have been studied especially for lithium specie due to its promising application for electrodes in lithium batteries [16], [17], [18]. Previously, a study on Na doped VSe_2 has been carried out [19]. Ekvall *et al.* measured a different CDW on the intercalated VSe_2 with a periodicity of 6.8 Å$\times$ 9.9 Å, which nearly

corresponds to a (2×3) superstructure, given a lattice parameter of 3.3 Å for VSe_2. Recent progress in the preparation of atomically thin TMD layers enables the growth of VSe_2 monolayers, in which a unique CDW symmetry of ($\sqrt{3} \times \sqrt{7}$) periodicity [10], notably different from the bulk phase, was discovered. The link between alkali-intercalated bulk VSe_2 and monolayer VSe_2 is still currently lacking. Here, we investigate Na-intercalated VSe_2 by combining scanning tunneling microscopy and spectroscopy (STM/STS) experiments and *ab initio* calculations. We compare and elucidate the electronic structures of pristine VSe_2 and the Na-intercalated areas. We show that Na intercalation induces a transition of the very top VSe_2 layer from the bulk CDW to the monolayer ($\sqrt{3} \times \sqrt{7}$) CDW, regardless of charge doping. In addition we observe a scanning tunneling spectroscopy (STS) local density of state (DOS) peak at the Fermi level at the frontier of non-intercalated areas. This peak shows an anomalous upward shift in energy, in contrast to the expected n-doping. We attribute this to a near-field gating effect due to charge redistribution induced by Na intercalation.

2 Results and Discussion

2.1 Pure VSe_2

The surface of bulk VSe_2 around 4 K exhibits a superstructure with a periodicity of 1.2 nm that corresponds to the known 4 × 4 bulk CDW (Figure 1a, inset). The dI/dV spectrum shown in Figure 1a exhibits three peaks. The first peak centered around -60 mV has a tail crossing the Fermi level, which is indicative of a band crossing the Fermi level and leads to metallic character of VSe_2. The second peak is located at +0.76 V and the third peak is accompanied by a plateau at around 2 V. These values are statistical averages from multiple measurements by different tips. The first two peaks correspond to previously reported spectra [20, 21]. The peak crossing the Fermi level has significant contribution from the vanadium *d* states based on tight binding [21] and various band structure calculations [19]. In order to reach a more detailed identification of this spectroscopic feature we have performed density functional theory (DFT) calculations on three-monolayer VSe_2 with a (4x4) unit cell. The corresponding total DOS is represented in Figure 1b. We can observe similar peak features as those measured in STS, and in particular the peak crossing the Fermi level. A more detailed analysis of the contributions from different orbitals is represented in Figure 1c through the projected DOS (PDOS) on the vanadium *d* orbitals. Unlike the conventional axis used for 1T-phase TMD [22] along the metal-ligand bonds in an octahedron crystal field, we choose the TMD out-of-plane direction as the z axis, in order to better understand the interaction with the intercalated sodium atoms in the second part of this work. According to crystal field theory, a splitting of the *d* states is induced by the coordination of the metal atom with the surrounded chalcogen ligands. In the T-phase, an ideal octahedral environment should lead to a low energy three-fold degenerate t_{2g} state and a high energy two-fold degenerate e_g state [23]. However, in our chosen coordinates, the split orbitals are more similar to the conventional crystal field splitting in a 1H-type TMD monolayer. This is because VSe_2 is known to show a larger ratio ≈ 1.827 than the ideal c/a ratio of 1.633 (c: interlayer spacing, a: in-plane lattice constant) [24]. The local environment of V atom is thus trigonal antiprismatic like, and the splittings for trigonal prismatic (1H) and trigonal antiprismatic are similar. Note that a deviation from the octahedral geometry is also found in the case of a monolayer, therefore a similar splitting is also expected in that case (Fig. S1 Supporting Information).
In the energy range considered here, the LDOS is dominated by the vanadium *3d* orbital. As such, the orbital decomposition shows that the peak crossing the Fermi level is mainly composed of the vanadium d_{z^2} state. The second peak around 1 eV has a d_{z^2}, d_{xy} and $d_{x^2-y^2}$ character, while the third peak above 2 eV is made of d_{xz} and d_{yz} orbitals. This result is consistent with the trigonal anti-prismatic crystal field splitting. The corresponding bandstructure shown in Fig. S2 (Supporting Information) is consistent with previously reported angle resolved photoemission spectroscopy [25]. The PDOS reported in Figure 1c reveals doubly degenerated bands and one non degenerate band. This is due to a splitting of the t_{2g} state into a two-fold degenerate band (d_{xy}, $d_{x^2-y^2}$) and a d_{z^2} band. The d_{z^2} band crossing the Fermi level is expected to be quite sensitive to interlayer interactions due to its extended orbital shape

along the out-of-plane direction. Therefore, the intercalation of foreign dopants is expected to realize band engineering in this material, and more specifically to have an important effect on the peak crossing the Fermi level.

2.2 Na doped VSe_2

In order to investigate the effect of alkali intercalation on the vanadium d_{z^2} band and on the electronic properties of VSe_2, we have deposited Na atoms on the VSe_2 surface at room temperature. The entire procedure was carried out under ultra-high vacuum, which avoided any reaction of Na with air or moisture. This procedure leads to the formation of Na-intercalated islands on the sample, as seen in Figure 2a. The atom resolved images on top and out of such islands reveal the atomic lattices of VSe_2 as also shown from the images and their Fourier Transform (Fig.2b-e). This is indicative that the islands correspond to intercalated Na, in agreement with previous report [19].
In addition to the atomic resolution, corresponding to the Se atoms, the external-to-islands STM images reveal a superstructure of (4×4) periodicity with respect to the atomic lattice (Fig.2b). These two periodic features can be clearly seen in the Fourrier transform (Fig. 2c). This (4×4) pattern corresponds to the known CDW pattern of bulk VSe_2. On the intercalated areas, a new CDW order appears with a unit cell of 5.85 Å × 8.28 Å with a small tilt angle of 16° with respect to the atomic lattice. Considering the VSe_2 lattice parameter of 3.3 Å, this periodicity corresponds to a $(\sqrt{3} \times \sqrt{7})$ pattern (see Figure 2d). This periodicity and symmetry correspond exactly to the CDW of VSe_2 monolayers grown on HOPG, bilayer graphene on SiC, and even MoS_2 recently reported [10, 12]. Therefore, the intercalation of Na layer induces a similar transition of the CDW pattern from the bulk state to the monolayer state. This indicates the observed layer-dependent CDW symmetry is more affected by interlayer coupling, rather than from the charge of metal cations.
STS studies of the Na-intercalated island reveal finer details (Fig. 3a). On the intercalated VSe_2 area, the peak around the Fermi level shifts downward below the Fermi level to -160 mV, exhibiting nearly a cutoff at the Fermi level. This feature indicates a full filling of this d_{z^2} band. Since the observation of CDW modification suggests that the intercalated VSe_2 behaves like a monolayer, we have compared the spectroscopy of intercalated VSe_2 with a monolayer of VSe_2 grown on bilayer graphene on SiC(0001), (see Fig.S3 in SI). The dI/dV spectra of such pristine and Na-intercalated VSe_2 monolayers are shown in Fig. 3a along with the bulk VSe_2 STS for comparison (The corresponding STM image of the VSe_2 monolayer is shown in the supporting information). Interestingly, the spectroscopy around the Fermi level of the monolayer shows a similar feature as the Na intercalated VSe_2, i.e. a shift of the peak toward lower energy, reduced DOS at the Fermi level, with sometime a sharp cutoff (cf. Fig.3a). This indicates the similarity between monolayer VSe_2 and Na-intercalated top VSe_2 layer.
In order to gain more insight into this system, we have performed DFT calculations on the VSe_2 monolayer and on the Na intercalated VSe_2 trilayers. We then calculated the corresponding DOS to compare them to the one of pristine VSe_2 trilayer previously calculated. The structure model of the Na-intercalated VSe_2 is shown in Figure 3b and its corresponding projected DOS in Figure 3c. In all cases, the DOS presents the same general features, namely a peak crossing the Fermi level, a broad peak located around 1 eV and a peak above 2 eV. In the Na-intercalated case, the DOS is globally downshifted, which is indicative of a n-type doping due to electron transfer from Na to VSe_2. This charge transfer has been evaluated considering the Löwdin charges calculated with Fireball [26], yielding about 0.2 electrons transferred from each Na atom to VSe_2 . Note that in STM experiments we are unable to determine the exact V/Na stoichiometric ratio of the Na island area. In our model calculation, we put one Na per VSe_2 formula unit cell. However, tests of several Na structures all lead to similar trend though with slightly different charge transfer per Na.
The Na island intercalated between two VSe_2 layer is also simulated in DFT by considering a bottom bilayer of 2×50 unit cells in the *xy* plane, with a monolayer 2×51 unit cell on top. Between this top layer and the bilayer, a partial layer of Na atoms is intercalated. This configuration is chosen in order to allow the top layer to have the flexibility to relax atop the Na island. This optimized configuration is represented in Figure 3d. From this calculation, we have determined the charge transfer from each Na atom

to each VSe_2 unit cell in the top layer, which allows one to follow the profile evolution of this charge transfer along the Na island and the pristine VSe_2. This evolution along the y axis is represented in Figure 3e. The Na intercalated part exhibits an excess of electron charges with respect to the rest of the cell, bearing out the charge transfer from the Na atoms to the top layer. Also, we can observe that, as expected, the charge transfer drops back to zero when leaving the Na island to the pristine VSe_2. This is in agreement with the previously discussed experimental observation of a n-type doping of the top VSe_2 layer. As such, we recover the expected standard behavior in the bulk pristine VSe_2.

A more detailed comparison of the calculated DOS reveals that Na intercalated VSe_2 and the monolayer VSe_2 have the same single d_{z^2} peak structure, while this peak is split for the VSe_2 bulk case due to the interlayer coupling. Therefore, Na intercalation appears to decouple the bottom VSe_2 layers and the n-doped top VSe_2 layer. As a consequence, the doping shifts the d_{z^2} down in energy, below the Fermi level, and the decoupling turns the CDW pattern from the bulk (4×4) to the monolayer $(\sqrt{3} \times \sqrt{7})$ pattern.

Interestingly, at the edge of Na islands, we observe several unexpected spectroscopic features (cf. Fig.4a). A series of spectra has been measured across an island along a line (Fig. 4b) and is represented in a color coded 2D map in Fig. 4c. The first feature is that d_{z^2} peak crossing the Fermi energy has a more significant downward shift deep inside the Na-intercalated area, as compared to those near the island boundary. This can be observed from the convex shape (yellow line) between the island boundaries (dashed lines) in Fig. 4c. As a comparison, the peak at ≈0.8 V does not show this behavior. The second feature is that while the d_{z^2} peak position is less downward shifted as it moves toward the island boundary from the island internal region, a notable enhancement of the d_{z^2} peak intensity is noted (pointed by the two arrows in Fig. 4c at x ≈ 8 nm and x ≈ 17 nm) when the d_{z^2} peak position is at exactly the Fermi energy. To obtain detailed distribution of the peak positions in addition to the informative Fig. 4c, a histogram is shown in Fig. 5. In this plot, the histograms of peaks at ≈ 0 V and 0.8-1.0 V are assembled for four cases: (1) on no-Na bulk VSe_2; (2) on Na-intercalated area; (3) on the frontier edge of N-intercalated area; (4) on pristine monolayer VSe_2 (on a separate sample). The histogram reveals two interesting facts. First, (2) and (4) consist one set showing the statistical effect of Na intercalation is to downward shift (n-dope) the monolayer VSe_2 DOS. Second, (1) and (3) consist another set showing at the "edge" the DOS peak position histogram is upward shift (p-doped) with respect to the undoped VSe_2 bulk. From the similarity of histograms of cases (1) and (3), we argue the case (3) histogram represents the frontier region of the non intercalated VSe_2 bulk near the Na islands. Together with the upward shifted profile of the d_{z^2} peak position inside the Na island region, a specific effect near the edge of the Na island is suggested.

Figure 4e shows a conductance map very close to Fermi energy of a region shown in Fig. 4d. The upper right part is an unintercalated area, and the rest a Na intercalated island. The conductance is lower on the Na intercalated VSe_2 monolayer than on the non-intercalated bulk VSe_2, reflecting the down-shift of the peaks due to Na which induces a lowering of the dI/dV signal at the Fermi level. However, bright lines along the edge reflect can be observed, which reflect the peak upward shift that appears at the boundary between the pristine and the Na intercalated parts.

The upward shift of LDOS indicates an apparent "p-doping" at the edge. It is anomalous since Na donates charge to VSe_2, as shown in Fig. 3e. We argue as a possible explanation that the aforementioned specific edge effect is due to near-field electrostatic gating at the Na island edge. To explore this effect, we construct a Na-intercalated trilayer model similar to Fig. 3d. The model as shown in Fig. 6a, has a smaller unit cell (20×1) in the xy plane, and 7 Na atoms per unit cell. In contrast to Fig. 3e which shows the total charge transfer to the top VSe_2 layer, it examines closer the distribution of potential change before and after Na intercalation inside the VSe_2 layer. Note that a peculiar distortion appears in our optimized unit cell, which is not observed experimentally. This distortion might be originated from our specific choice of unit cell, very long in order to observe distinctly the phases with and without Na. However, since the main physical behavior of doping of vanadium by the sodium atoms has been caught in this model and the evolution of the d orbital shift with the electronic doping is in correct agreement with the experimental results, we do not think it has a strong influence on the observed results. In Fig. 6b, the cyan and yellow color denotes regions nearer positive and negative transferred charge,

respectively. One can observe each atom in the top VSe_2 layer is polarized by the Na cations and the shape around each atom is like a dipole potential distribution. Interestingly, the atomic dipole potential axis (marked with arrows) gradually tilt from the out-of-plane direction toward the in-plane direction as they move outward and across the Na island edge. Therefore, an in-plane component of the electric field appears at the edge of the island. This in-plane electric field induces a shift of the d_{z^2} state due to the Stark effect, that occurs only at the edge.

3 Conclusion

To summarize, we present here an STM study of sodium intercalation in a pristine bulk VSe_2. Sodium atoms are deposited on the pristine VSe_2 and they intercalate between the top layer and the rest bulk layer. As a result, the (4× 4) CDW VSe_2 pattern observed in the pristine phase turns into a ($\sqrt{3} \times \sqrt{7}$) CDW pattern, which is identical to the CDW observed in monolayer VSe_2 grown on several substrates. The STS measured for Na-doped VSe_2 are similar to those of pristine VSe_2 monolayer and bulk, but show subtle differences. DFT calculations indicate a significant charge transfer between sodium atoms and the top VSe_2 layer (n-doping), and reveals that sodium intercalation decouples the two VSe_2 top layers. This doping results in a shift down to the negative energies of the d_{z^2} vanadium orbitals. The Na-intercalation changes the interlayer coupling and endows the top VSe_2 layer the same $\sqrt{3} \times \sqrt{7}$ VSe_2 monolayer CDW order. However, an anomalous and reverse p-doping behavior is observed near the Na island boundary, as a result of electrostatic local gating by the transferred negative charge and its distribution. From these results, we believe that the main origin of the CDW change is a strong electronic modification due to electronic doping and change of interlayer coupling. The determination of their relative importance on Fermi surface nesting and electron-phonon coupling, and the coupling between lattice distortion and electronic structure will be the subject of a future work. Finally, this work shows how alkali intercalation can be used to induce a transition of the VSe_2 CDW from the bulk to the monolayer phase and to render unexpected inhomogeneity in doping. This opens new routes to tune the properties of TMDs exhibiting CDWs.

Experimental Section

VSe_2 bulk crystals were grown by CVT in furnaces. A piece of VSe_2 crystal was glued onto an omicron sample plate and then cleaved first in air and then in vacuum to avoid air contamination on the surface. The doping was conducted with a SAES Na getter source. We exposed the VSe_2 crystal in situ to pure Na vapor for 30 min at a pressure of 1.5×10^{-9} mbar at room temperature. Such a doping condition corresponds to the deposition of 0.5 ML Na. We investigated our sample using low temperature STM and STS at 4 K, with a base pressure better than 3×10^{-10} mbar. STM topography image were obtained in constant current mode unless specified otherwise and the bias voltage was applied to the sample. Tungsten tips are home-made by electrochemical etching. STS measurements were done at a modulation frequency of 746 Hz. Results were cross-checked and found consistent in two LT-STM systems at 4 K and 78 K. The monolayer VSe_2 on SiC was prepared by MBE with a base pressure of 1.5×10^{-9} mbar. Selenium atoms were evaporated from a Knudsen cell and vanadium flux was produced by an Omicron EFM3 evaporator. The flux ratio of V/Se was set at 1:10 as calibrated by a quartz crystal microbalance.

Density Functional Theory (DFT) calculations, except that of Fig. 6, have been performed using an efficient DFT localized-orbital molecular-dynamics code as implemented in Fireball [27, 26, 28, 29]. In particular, it has been used to optimize the three-monolayer VSe_2 (4x4) structure, with or without sodium intercalation, and to determine the corresponding electronic structures. To this end, the structure has been optimized (keeping the bottom VSe_2 layer fixed in order to simulate the bulk below the three monolayers) until the forces went below 0.1 eV/Å. A set of 8 × 8× 1 k-points has been used for both structural optimization and density of states (DOS) or charge transfer calculations.

The DFT calculations of Fig. 6 were performed by using plane-wave based software Vienna ab-initio simulation package (VASP) [30, 31]. To mimic a Na-intercalation step structure, we used a 20×1 VSe_2 supercell with three VSe_2 layers. The bottom VSe_2 layer was fixed to its bulk geometric and the rest atoms were allowed to relax. The energy cutoff of 520 eV for the plane-wave basis and $1\times7\times1$ Monkhorst-Pack [32] gamma-centered k-point meshes for the Brillouin zone were used for the geometric and electronic calculations. The exchange-correlation functional was treated in the generalized gradient approximation with the Perdew–Burke–Ernzerhof (PBE) functional [33]. The electronic configuration of Na, V, and Se in the VASP pseudopotentials are $2s^2 2p^6 3s^1$, $3d^4 4s^1$, and $4s^2 4p^4$, respectively. The semi-empirical van der Waal correction of Grimme (vdW-D3) was used [34] to describe the weak dispersion forces. The energy and force converged criterion are set to 10^{-5} eV and 0.01 eV/Å, respectively. For the potential distribution plots, the ionic and Hartree potentials were included and the exchange-correlation potential was excluded since it decays rather slowly in the vacuum region.

Supporting Information
Supporting Information is available from the Wiley Online Library or from the author.

Acknowledgements
We thank the French National Research Agency (ANR-20-CE09-0023 DEFINE2D project) and Taiwan MOST (111-2923-M-002-011- DEFINED2D project) for support. Dr. W. W. Pai also acknowledge the support by MOST 110-2112-M-002-040-MY3 and AIMAT. R.S. acknowledges the financial support provided by the Ministry of Science and Technology in Taiwan under Project No. MOST-110-2112-M-001-065-MY3 and Academia Sinica budget of AS-iMATE-111-12

References

[1] G. Liu, B. Debnath, T. R. Pope, T. T. Salguero, R. K. Lake, A. A. Balandin, *Nat. Nanotechnol.* **2016**, *11*, 10 845.

[2] I. Vaskivskyi, I. A. Mihailovic, S. Brazovskii, J. Gospodaric, T. Mertelj, D. Svetin, P. Sutar, D. Mihailovic, *Nat. Commun.* **2016**, *7*, 1 11442.

[3] K. Rossnagel, *J. Phys.: Condens. Matter* **2011**, *23* 213001.

[4] J. Li, L. Jiang, W. Ma, T. Wu, Q. Qiu, Y. Shi, W. Zhou, N. Yao, Z. Huang, *ACS Applied Nano Materials* **2022**, *5* 5158.

[5] W. Feng, M. Cheng, R. Du, Y. Wang, P. Wang, H. Li, L. Song, X. Wen, J. Yang, X. Li, J. He, J. Shi, *Adv. Mater. Interfaces* **2022**, *9*, 13 2200060.

[6] M. Salavati, T. Rabczuk, *Comput. Mater. Sci.* **2019**, *160* 360.

[7] K. Terashima, T. Sato, H. Komatsu, T. Takahashi, N. Maeda, K. Hayashi, *Phys. Rev. B* **2003**, *68* 155108.

[8] Z. Wang, J. Zhou, K. P. Loh, Y. P. Feng, *Appl. Phys. Lett.* **2021**, *119* 163101.

[9] J. G. Si, W. J. Lu, H. Y. Wu, H. Y. Lv, X. Liang, Q. J. Li, Y. P. Sun, *Phys. Rev. B* **2020**, *101* 235405.

[10] P. Chen, W. W. Pai, Y.-H. Chan, V. Madhavan, M.-Y. Chou, S.-K. Mo, A.-V. Fedorov, T.-C. Chiang, *Phys. Rev. Lett.* **2018**, *121* 196402.

[11] M. Bonilla, S. Kolekar, Y. Ma, H. C. Diaz, V. Kalappattil, R. Das, T. Eggers, H. R. Gutierrez, M.-H. Phan, M. Batzill, *Nat. Nanotechnol.* **2018**, *13* 289.

[12] P. M. Coelho, K. Nguyen Cong, M. Bonilla, S. Kolekar, M.-H. Phan, J. Avila, M. C. Asensio, I. I. Oleynik, M. Batzill, *J. Phys. Chem. C* **2019**, *123* 14089.

[13] W. Yu, J. Li, T. S. Herng, Z. Wang, X. Zhao, X. Chi, W. Fu, I. Abdelwahab, J. Zhou, J. Dan, Z. Chen, Z. Chen, Z. Li, J. Lu, S. J. Pennycook, Y. P. Feng, J. Ding, K. P. Loh, *Adv. Mater.* **2019**, *31* 1903779.

[14] W. Zhang, L. Zhang, P. K. J. Wong, J. Yuan, G. Vinai, P. Torelli, G. van der Laan, Y. P. Feng, A. T. S. Wee, *ACS Nano* **2019**, *13* 8997.

[15] R. Chua, J. Yang, X. He, X. Yu, W. Yu, F. Bussolotti, P. K. J. Wong, K. P. Loh, M. B. H. Breese, K. E. J. Goh, Y. L. Huang, A. T. S. Wee, *Adv. Mater.* **2020**, *32* 2000693.

[16] C. Yang, J. Feng, F. Lv, J. Zhou, C. Lin, K. Wang, Y. Zhang, Y. Yang, W. Wang, J. Li, S. Guo, *Adv. Mater.* **2018**, *30* 1800036.

[17] H. Ci, J. Cai, H. Ma, Z. Shi, G. Cui, M. Wang, J. Jin, N. Wei, C. Lu, W. Zhao, J. Sun, Z. Liu, *ACS Nano* **2020**, *14* 11929.

[18] F. Ming, H. Liang, Y. Lei, W. Zhang, H. N. Alshareef, *Nano Energy* **2018**, *53* 11.

[19] I. Ekvall, H. E. Brauer, E. Wahlström, H. Olin, *Phys. Rev. B* **1999**, *59* 7751.

[20] r. Pásztor, A. Scarfato, C. Barreteau, E. Giannini, C. Renner, *2D Mater.* **2017**, *4* 041005.

[21] W. Jolie, T. Knispel, N. Ehlen, K. Nikonov, C. Busse, A. Grüneis, T. Michely, *Phys. Rev. B* **2019**, *99* 115417.

[22] D. Pasquier, O. V. Yazyev, *2D Mater.* **2019**, *6* 025015.

[23] E. Benavente, M. Santa Ana, F. Mendizábal, G. González, *Coordin. Chem. Rev.* **2002**, *224* 87.

[24] G. A. Wiegers, *J. Phys. C* **1981**, *14* 4225.

[25] J. Feng, D. Biswas, A. Rajan, M. D. Watson, F. Mazzola, O. J. Clark, K. Underwood, I. Marković, M. McLaren, A. Hunter, D. M. Burn, L. B. Duffy, S. Barua, G. Balakrishnan, F. Bertran, P. Le Fèvre, T. K. Kim, G. van der Laan, T. Hesjedal, P. Wahl, P. D. C. King, *Nano Lett.* **2018**, *18*, 7 4493.

[26] P. Jelínek, H. Wang, J. P. Lewis, O. F. Sankey, J. Ortega, *Phys. Rev. B* **2005**, *71* 235101.

[27] J. P. Lewis, P. Jelínek, J. Ortega, A. A. Demkov, D. G. Trabada, B. Haycock, H. Wang, G. Adams, J. K. Tomfohr, E. Abad, H. Wang, D. A. Drabold, *Phys. Status Solidi B* **2011**, *248* 1989.

[28] O. F. Sankey, D. J. Niklewski, *Phys. Rev. B* **1989**, *40* 3979.

[29] M. Basanta, Y. Dappe, P. Jelínek, J. Ortega, *Comp Mater Sci* **2007**, *39* 759.

[30] G. Kresse, J. Hafner, *Phys. Rev. B* **1993**, *47* 558.

[31] G. Kresse, J. Furthmüller, *Phys.Rev. B* **1996**, *54* 11169.

[32] H. J. Monkhorst, J. D. Pack, *Phys. Rev. B* **1976**, *13* 5188.

[33] J. P. Perdew, K. Burke, M. Ernzerhof, *Phys. Rev. lett.* **1996**, *77* 3865.

[34] S. Grimme, J. Antony, S. Ehrlich, H. Krieg, *J. Chem. Phys.* **2010**, *132*, 15 154104.

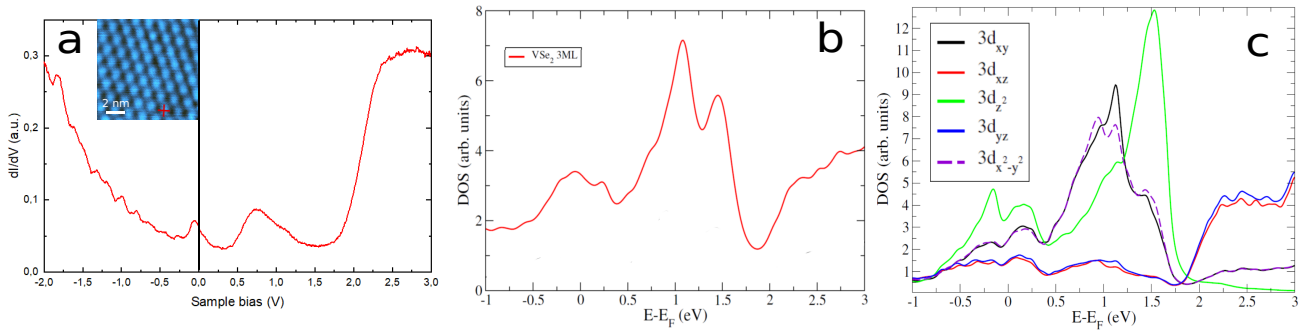

Figure 1: (a) Pure VSe_2 spectrum taken at the red cross position in the inset. Inset : Constant current image of the (4 × 4) CDW on VSe_2 (V=0.5V, I=50pA) . This STS shows three VSe_2 peaks which orbitals are identified with the DFT calculations. (b) Total DOS of a 1T-phase VSe_2 3-monolayers (4x4 unit cell); (c) Projection of d orbitals of the total DOS. The z axis is chosen along the direction perpendicular to the TMD plane.

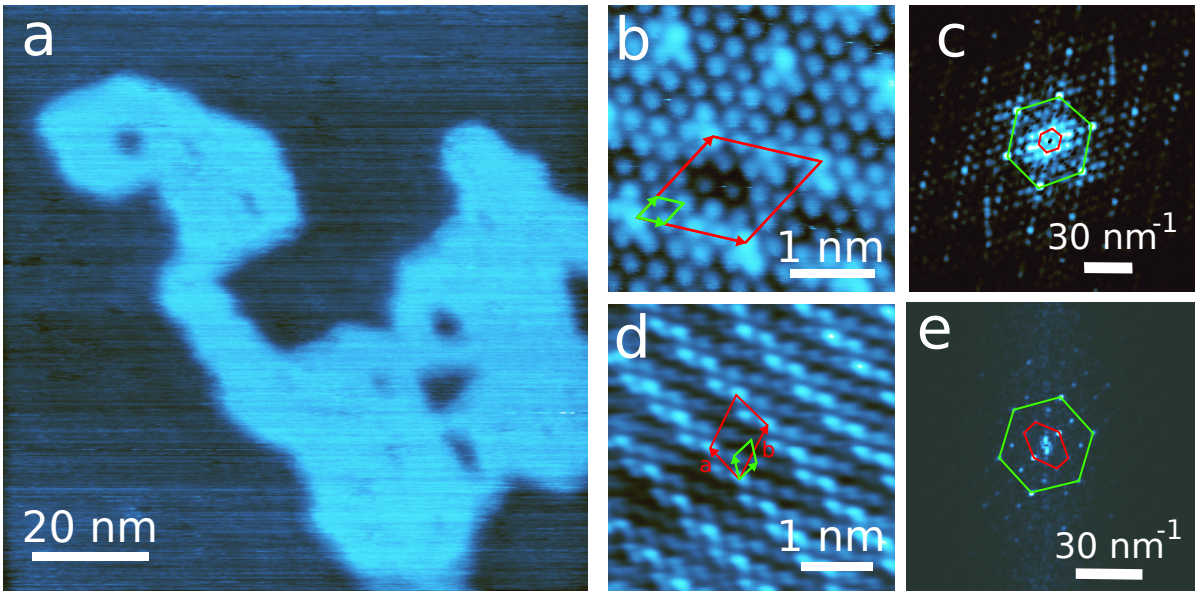

Figure 2: (a) Constant current image of a Na island on VSe_2 (V=1V, I=20 pA) ; (b) Constant current image of the (4 × 4) VSe_2 CDW (V=0.6mV, I=2.7nA) and (c) Fourier Transform of (b) ; (d) Constant current image of the ($\sqrt{3}$ × $\sqrt{7}$) CDW on top of the island (V=1V, I=50pA); (e) Fourier Transform of (d)

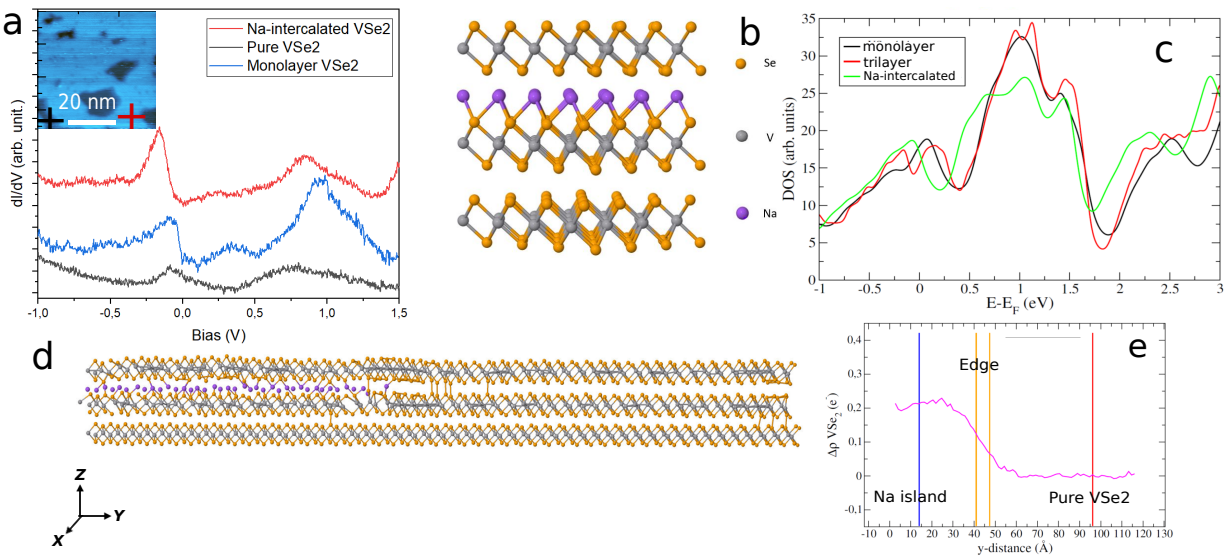

Figure 3: (a) STS spectrum between -1V and 1.5V on three different area for comparison. On Na-intercalated layer (red cross on the inset), on non intercalated VSe_2 (black cross on the inset) and on monolayer VSe_2. Inset : Constant current image of Na island (V=1V, I=100pA). The Na island STS first peak shifts downward as would the one for the monolayer. (b) Unit cell of intercalated sodium in VSe_2 3 layers. (c) Total DOS of the Na VSe_2 cell (green) compared with the previous total DOS of pure T phase VSe_2 trilayers (red) and the pure 1T- VSe_2 monolayer (black). (d) 2 $\times$ 50 trilayer intercalated $NaVSe_2$ unit cell. (e) Charge difference with respect to the undopped VSe_2 lattice across the junction displayed in (d).

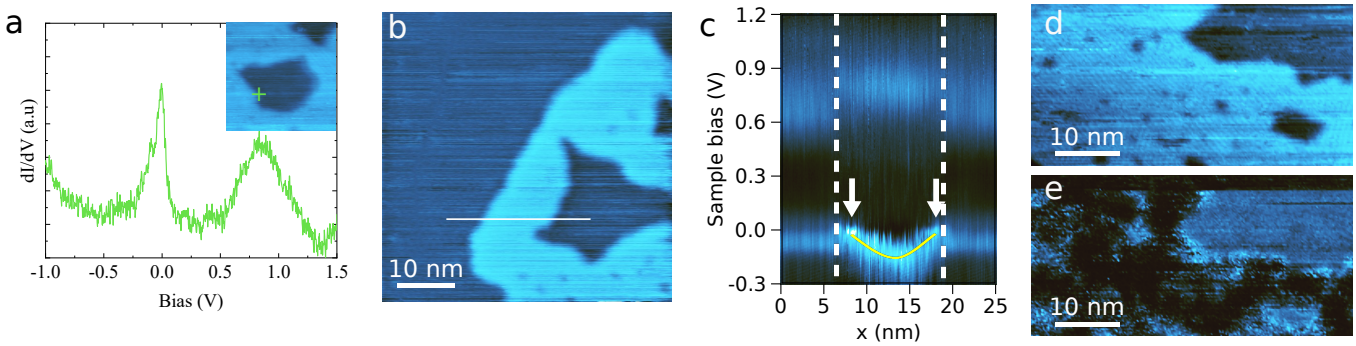

Figure 4: (a) STS taken on the Na island edge point indicated by the green cross in the inset (V=1V, I=100pA) ; (b - c) Constant current image of an Na island (V=1V, I=400pA) and (c) the 1D conductance map along the corresponding line on (b) ; (d - e) Constant current image of a Na island (V=1V, I=200pA) and its corresponding conductance map at a bias of 12mV on the same area.

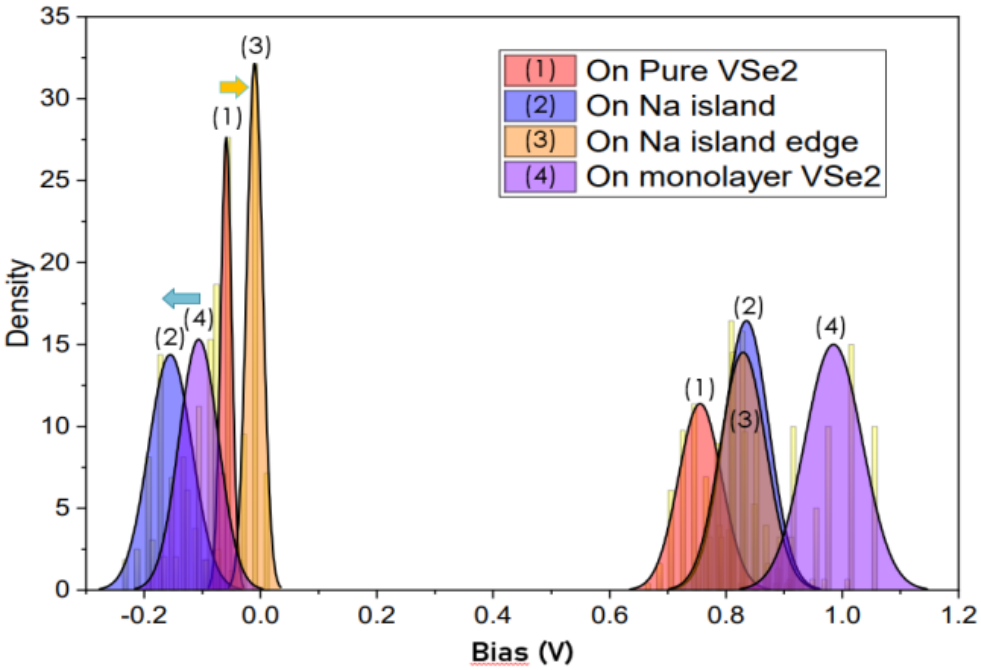

Figure 5: Statistics of the two $3d$ derived peaks in the measured STS on different areas. The two arrows show doping behavior, respectively p-type (orange arrow) and n-type (blue).

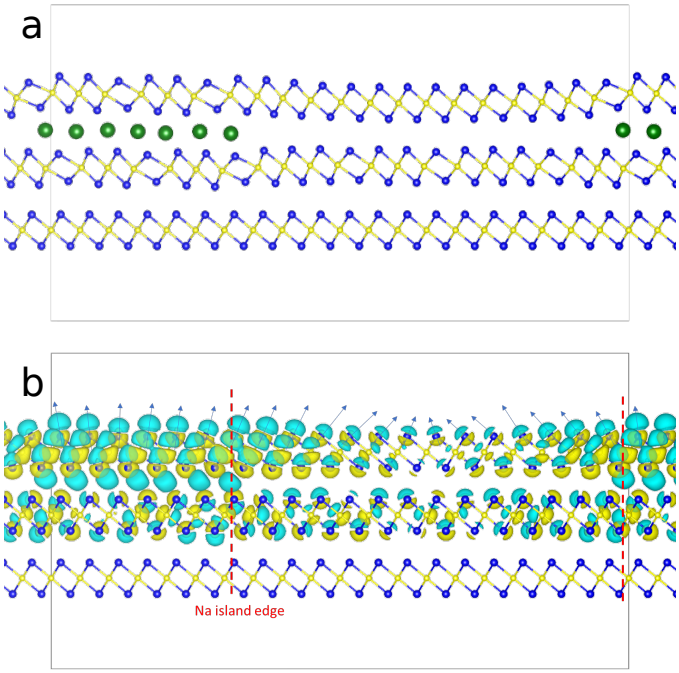

Figure 6: (a) 1×20 cell representing the Na-intercalated VSe_2 ; (b) potential difference 3D isosurface plot for an isovalue of 5. The cyan- and yellow- colored lobes represent negative and positive isovalues respectively. The red dotted lines show the edge of Na island. The blue thin arrows indicate the axes of top layer dipoles.

Table of Contents

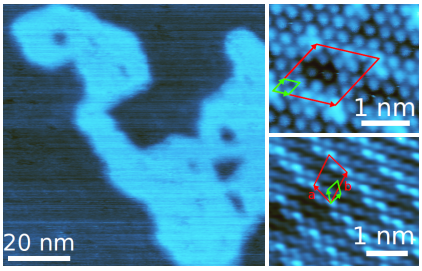

Na islands have been intercalated in bulk VSe2. Combining scanning tunneling micrscopy experiments and ab-initio calculations, the charge density wave is found to switch from the bulk phase to the monolayer phase when Na is intercalated. At the edge of the Na island a p-like doping is observed.